Direct Substrate Delivery Into Mitochondrial Fission–Deficient Pancreatic Islets Rescues Insulin Secretion

Uma D. Kabra,[1,2,3] Katrin Pfuhlmann,[1,2,3] Adriana Migliorini,[1,2] Susanne Keipert,[1,2] Daniel Lamp,[1,2,3] Olle Korsgren,[4] Moritz Gegg,[1,2,3] Stephen C. Woods,[5] Paul T. Pfluger,[1,2] Heiko Lickert,[1,2,3] Charles Affourtit,[6] Matthias H. Tschöp,[1,2,3] and Martin Jastroch[1,2]

Diabetes 2017;66:1247–1257 | DOI: 10.2337/db16-1088

In pancreatic β-cells, mitochondrial bioenergetics control glucose-stimulated insulin secretion. Mitochondrial dynamics are generally associated with quality control, maintaining the functionality of bioenergetics. By acute pharmacological inhibition of mitochondrial fission protein *Drp1*, we demonstrate in this study that mitochondrial fission is necessary for glucose-stimulated insulin secretion in mouse and human islets. We confirm that genetic silencing of *Drp1* increases mitochondrial proton leak in MIN6 cells. However, our comprehensive analysis of pancreatic islet bioenergetics reveals that *Drp1* does not control insulin secretion via its effect on proton leak but instead via modulation of glucose-fueled respiration. Notably, pyruvate fully rescues the impaired insulin secretion of fission-deficient β-cells, demonstrating that defective mitochondrial dynamics solely affect substrate supply upstream of oxidative phosphorylation. The present findings provide novel insights into how mitochondrial dysfunction may cause pancreatic β-cell failure. In addition, the results will stimulate new thinking in the intersecting fields of mitochondrial dynamics and bioenergetics, as treatment of defective dynamics in mitochondrial diseases appears to be possible by improving metabolism upstream of mitochondria.

The development of type 2 diabetes is associated with mitochondrial dysfunction in pancreatic β-cells. β-Cells have developed highly coordinated mechanisms that link glucose sensing with metabolic signaling cascades that direct the secretion of sufficient insulin to maintain glucose homeostasis (1). The mechanism underlying glucose-stimulated insulin secretion (GSIS) from β-cells involves glucose uptake by specific glucose transporters followed by glucose catabolism through glycolysis yielding pyruvate, which in turn is further catabolized via the tricarboxylic acid cycle. Both glycolysis and tricarboxylic acid cycle turnover generate reducing power that is used by the mitochondrial respiratory chain to produce ATP through oxidative phosphorylation. The resultant increase in the cytosolic ATP/ADP ratio closes ATP-sensitive K^+ (K_{ATP}) channels, thus depolarizing the plasma membrane. Depolarization triggers opening of voltage-gated Ca^{2+} channels, and the influx of Ca^{2+} ions consequently leads to exocytosis of insulin-containing granules from β-cells (2). This sequence of events illustrates that β-cell mitochondria exert strong control over GSIS (3), as mitochondrial energy-transducing processes dictate how fast and efficiently glucose is converted to ATP. Mitochondrial dysfunction impairs glucose–insulin secretion coupling and ultimately promotes β-cell apoptosis and death, one of the key features of type 2 diabetes (4).

Mitochondria are dynamic organelles that are constantly remodeled through the opposing action of fission and fusion proteins (5). Until recently, the influence of mitochondrial dynamics over energy transduction has been underappreciated. The continuous changes in mitochondrial morphology are controlled by a group of evolutionarily highly conserved

[1]Helmholtz Diabetes Center, Helmholtz Zentrum München, Neuherberg, Germany
[2]German Center for Diabetes Research, Helmholtz Zentrum München, Neuherberg, Germany
[3]Division of Metabolic Diseases, Technische Universität München, Munich, Germany
[4]Department of Immunology, Genetics and Pathology, Uppsala University, Uppsala, Sweden
[5]Department of Psychiatry and Behavioral Neuroscience, University of Cincinnati, Cincinnati, OH
[6]School of Biomedical and Healthcare Sciences, Plymouth University, Plymouth, U.K.

Corresponding author: Martin Jastroch, martin.jastroch@helmholtz-muenchen.de.

Received 8 September 2016 and accepted 29 January 2017.

This article contains Supplementary Data online at http://diabetes.diabetesjournals.org/lookup/suppl/doi:10.2337/db16-1088/-/DC1.

large GTPases of the dynamin superfamily (5). Mitochondrial fusion is regulated by mitofusins 1 and 2 (*Mfn1/2*) and optic atrophy 1 (*Opa1*), whereas mitochondrial fission is regulated by dynamin-related protein 1 (*Drp1*) and fission protein 1 (*Fis1*) (6). Increasing evidence suggests that a subtle balance between mitochondrial fission and fusion events is crucial for achieving the mitochondrial morphology required for a particular (energetic) function (7–9). Deficiencies in the proteins regulating mitochondrial dynamics have been associated with several human diseases including dominant optic atrophy for *Opa1*, Charcot-Marie-Tooth disease type 2A for *Mfn2*, and developmental defects for *Drp1* (10–12). Indeed, there is evidence that the pancreatic islets of patients with diabetes exhibit swollen and enlarged mitochondria, implying disturbed mitochondrial morphology under diabetic conditions (13).

The GTPase gene *Drp1* is considered pivotal for regulating mitochondrial fission (14). In response to metabolic demand, *Drp1* translocates from the cytoplasm to the mitochondrial surface, where it forms a complex with *Fis1*. Oligomerization of *Drp1* provides the mechanical force required to constrict the mitochondrial membranes and thereby facilitate fission (15). Recent studies suggest that *Drp1* recruitment involves posttranslational modifications including sumoylation, *S*-nitrosylation, ubiquitination, and phosphorylation (16,17). Interestingly, *Drp1* activation under glucolipotoxic conditions in pancreatic β-cells leads to abnormalities in mitochondrial structure and function, followed by activation of proapoptotic signaling cascades (18–21). It has recently been reported that manipulation of mitochondrial morphology by overexpressing dominant-negative *Drp1* with erased GTPase activity decreases GSIS in INS-1E insulinoma cells, and this was attributed to increased mitochondrial proton leak (22). Collectively, these findings emphasize the important role of mitochondrial dynamics in pancreatic β-cell biology, although exact mechanisms have yet to be established firmly.

In the current study, we used genetic and pharmacological inactivation of *Drp1* to assess mechanistically how mitochondrial dynamics control mitochondrial energy transduction and subsequently how this affects GSIS in MIN6 cells and human and mouse pancreatic islets. We confirm that genetic silencing of the mitochondrial fission protein *Drp1* by use of lentivirus-mediated short hairpin RNA (shRNA) disrupts mitochondrial morphology and impairs GSIS in MIN6 cells. We demonstrate that the decrease of insulin secretion is secondary to a decreased ATP synthesis instead of increased mitochondrial proton leak, as suggested previously (22). We exclude long-term effects on autophagy and mitochondrial quality control by acute pharmacological inactivation of *Drp1* with the mitochondrial division inhibitor (mdivi-1). Mdivi-1 displays identical attenuating effects on GSIS in mouse and human pancreatic islets. Mechanistically, however, comprehensive real-time analysis of cellular respiration reveals that the deficient mitochondrial fragmentation lowers coupling efficiency of oxidative phosphorylation by decreasing glucose-fueled respiration and not by increasing proton leak. Because *Drp1* inhibition did not change respiratory complex subunit concentrations, we hypothesized that mitochondrial substrate supply may be hampered in fission-deficient pancreatic β-cells. Consistent with this, we reveal that direct supply of exogenous (methyl) pyruvate fully rescues deficits in oxidative phosphorylation, ATP output, and GSIS in fission-deficient cells and islets. This discovery of physiologically relevant impairments upstream of oxidative phosphorylation offers therapeutic options for treating mitochondrial dynamics–related β-cell dysfunction and associated metabolic diseases.

RESEARCH DESIGN AND METHODS

Human and Mouse Islets

Human islets were provided through JDRF award 31-2008-416 (European Consortium for Islet Transplantation [ECIT] Islets for Basic Research Program), and islet experiments were approved by the Ethical Commission of the Technical University of Munich (Munich, Germany). Mouse islets were isolated by collagenase digestion as previously described (23). For details on islet-culturing conditions, refer to the Supplementary Data.

MIN6 Cells and Viral Infection

For details on cell culture and viral conditions, refer to the Supplementary Data.

Insulin Secretion From Islets

Equal-number batches of islets were washed twice with HEPES-balanced Krebs-Ringer (KRH) bicarbonate buffer composed of 114 mmol/L NaCl, 4.7 mmol/L KCl, 2.5 mmol/L $CaCl_2$, 1.16 mmol/L $MgSO_4$, 1.2 mmol/L KH_2PO_4, 25.5 mmol/L $NaHCO_3$, and 20 mmol/L HEPES (pH 7.2–7.4), supplemented with 0.2% (weight for volume) BSA and 2 mmol/L glucose. The islets were starved in the same buffer with and without 100 μmol/L mdivi-1 for 1 h at 37°C. Later, starvation buffer was aspirated, and islets were incubated in KRH bicarbonate buffer with indicated concentrations of glucose and other secretagogues with and without 100 μmol/L mdivi-1 for 1 h at 37°C. Thereafter, the supernatants were collected and centrifuged at 760 × *g* for 5 min for determination of insulin concentration using a mouse ultrasensitive insulin ELISA kit (Alpco). Following the secretion assay, islets were washed twice with Dulbecco's PBS, and ice-cold RIPA lysis buffer was added. Islet homogenates were collected, centrifuged at 12,000 × *g* for 10 min, and assayed for total insulin content by radioimmunoassay. For normalization, DNA content was measured using the Quant-it Pico Green DNA assay kit (Invitrogen). Each independent experiment was performed with three technical replicates. Refer to the Supplementary Data for details on insulin secretion from MIN6 cells.

Cellular Bioenergetics

An extracellular flux analyzer XF24 (Seahorse Bioscience) was used to determine oxygen consumption rate. Cells were seeded into XF24-well plates at a density of 40,000 cells/well in DMEM containing 25 mmol/L glucose. The

cells were washed twice with bicarbonate-free KRH buffer containing 2 mmol/L glucose and starved in the same buffer with and without mdivi-1 for 2 h at 37°C in a non-CO_2 incubator. After recording basal cellular respiration, cells were treated sequentially with glucose (16.5 mmol/L) and other secretagogues, oligomycin (2 μg/mL), and eventually rotenone/antimycin A (1 and 2 μmol/L, respectively) to correct for nonmitochondrial respiration. Respiration values are presented after correction and normalization with DNA content. The respiratory data were analyzed and interpreted according to Divakaruni et al. (24). In short, "basal respiration" represents mitochondrial respiration rates at 2 mmol/L glucose, and "ATP-linked respiration" represents the respiration rates prior to injection of oligomycin minus oligomycin-insensitive rates. Oligomycin-insensitive rates are labeled "proton leak respiration." The coupling efficiency represents the fraction of respiration used to drive ATP synthesis for each run, calculated as CE = 1 − (proton leak/respiration prior to oligomycin injection).

Islet Bioenergetics

Batches of equal numbers of islets were plated into XF24-well islet culture plates and washed twice with bicarbonate-free KRH buffer supplemented with 2 mmol/L glucose. The islets were starved in the same buffer with and without 100 μmol/L mdivi-1 for 1 h at 37°C in a non-CO_2 incubator. The plate was then placed into the machine (controlled at 37°C) for a 10-min calibration followed by four measurement cycles to record basal cellular respiration. Islets were then treated sequentially with glucose (16.5 mmol/L), oligomycin (10 μg/mL), and a mixture of rotenone/antimycin A (both 2 μmol/L). Respiration values were calculated by subtracting nonmitochondrial respiration. For normalization, DNA content of the cells was measured.

Intracellular ATP Content

Cells were seeded into white 96-well plates at a density of 10,000 cells/well in DMEM containing 25 mmol/L glucose. Cells were treated similarly as for the insulin-secretion assay. At the end of experiment, medium was aspirated; cells were washed twice with ice-cold Dulbecco's PBS, and ATP content was determined using the Luminescent ATP detection assay kit (Abcam). Results were corrected for DNA content.

Glucose Uptake Assay, Western Blot Analysis, RNA Isolation, and Quantitative Real-time PCR

For details, refer to the Supplementary Data.

Mitochondrial Morphology

Mitochondrial morphology was examined in live nontarget and *Drp1* knockdown (KD) MIN6 cells stained with 40 nmol/L MitoTracker Red FM (Invitrogen) for 30 min. After three to five washes, cells were examined using an SP5 confocal microscope (Leica Microsystems) with a 60× objective lens.

Statistical Analysis

Data were collected from several independent experiments, and results are expressed as means ± SEM. Unpaired two-tailed Student *t* tests were used to compare two variables, and one-way ANOVA (with Bonferroni post hoc analysis) was used for multiple comparisons using Prism version 6.0 (GraphPad Software). Statistically significant differences were considered at $^{*}P < 0.05$, $^{**}P < 0.01$, and $^{***}P < 0.001$.

RESULTS

Drp1 KD Changes Mitochondrial Morphology and Decreases GSIS

MIN6 cells targeted with specific shRNA express ~50% less *Drp1* mRNA (Fig. 1*A*) and 80% less protein (Fig. 1*B*) than nontargeted control cells. *Drp1* KD did not affect *Mfn1* or *Opa1* mRNA levels but caused an increase in *Mfn2* mRNA, consistent with the concept that mitochondrial elongation is supported (Fig. 1*C*). Moreover, fluorescent visualization of the mitochondrial network revealed elongated mitochondria in *Drp1* KD cells (i.e., it demonstrated the expected morphological changes) (Fig. 1*D* and *E*). Western analysis of representative subunits from all respiratory complexes (gene names are found in Fig. 1*F*) confirms that *Drp1* KD does not affect the composition of the mitochondrial electron-transfer chain (Fig. 1*F*). Equally, *Drp1* KD leaves the insulin content of MIN6 cells unaffected (Fig. 1*G*), although it lowered Ins2 (not Ins1) mRNA (Fig. 1*H*).

Basal insulin release at 2 mmol/L glucose was not affected by *Drp1* KD, but insulin secretion at 16.5 mmol/L glucose was significantly decreased (Fig. 2*A*), strongly implicating mitochondrial dynamics in the control of nutrient-secretion coupling in pancreatic β-cells. *Drp1* KD did not affect insulin secretion mechanisms downstream of mitochondria, as neither KCl- nor glyburide-provoked insulin release was changed (Fig. 2*A*). In the presence of low glucose levels (2 mmol/L), potassium served to depolarize the plasma membrane, whereas glyburide, a sulfonylurea, specifically closes ATP-dependent potassium channels. These findings strongly suggest that *Drp1* KD decreases GSIS through deleterious effects on glucose catabolism.

Drp1 KD Lowers Coupling Efficiency of Oxidative Phosphorylation

Real-time oxidative breakdown of glucose can be followed readily in intact cells by measuring mitochondrial oxygen uptake using Seahorse technology (25). Using this plate-based respirometry platform, we measured basal respiratory activity of MIN6 cells, added glucose to monitor glucose-stimulated respiration, and inhibited the ATP synthase with oligomycin to estimate to what extent respiration is used to make ATP and how much of it is linked to mitochondrial proton leak. Figure 2*B* depicts typical oxygen consumption traces, corrected for nonmitochondrial respiration, for the entire time course of the respiratory assay. Calculations for (non)mitochondrial respiration, proton leak, ATP-linked respiration, and coupling efficiency are described in RESEARCH DESIGN AND METHODS. Low-glucose experiments (2 mmol/L) that did not require additional glucose during the assay were run in separate wells from high-glucose (16.5 mmol/L) experiments and carefully time-matched. Mitochondrial respiration at 2 and 16.5 mmol/L glucose was not significantly different

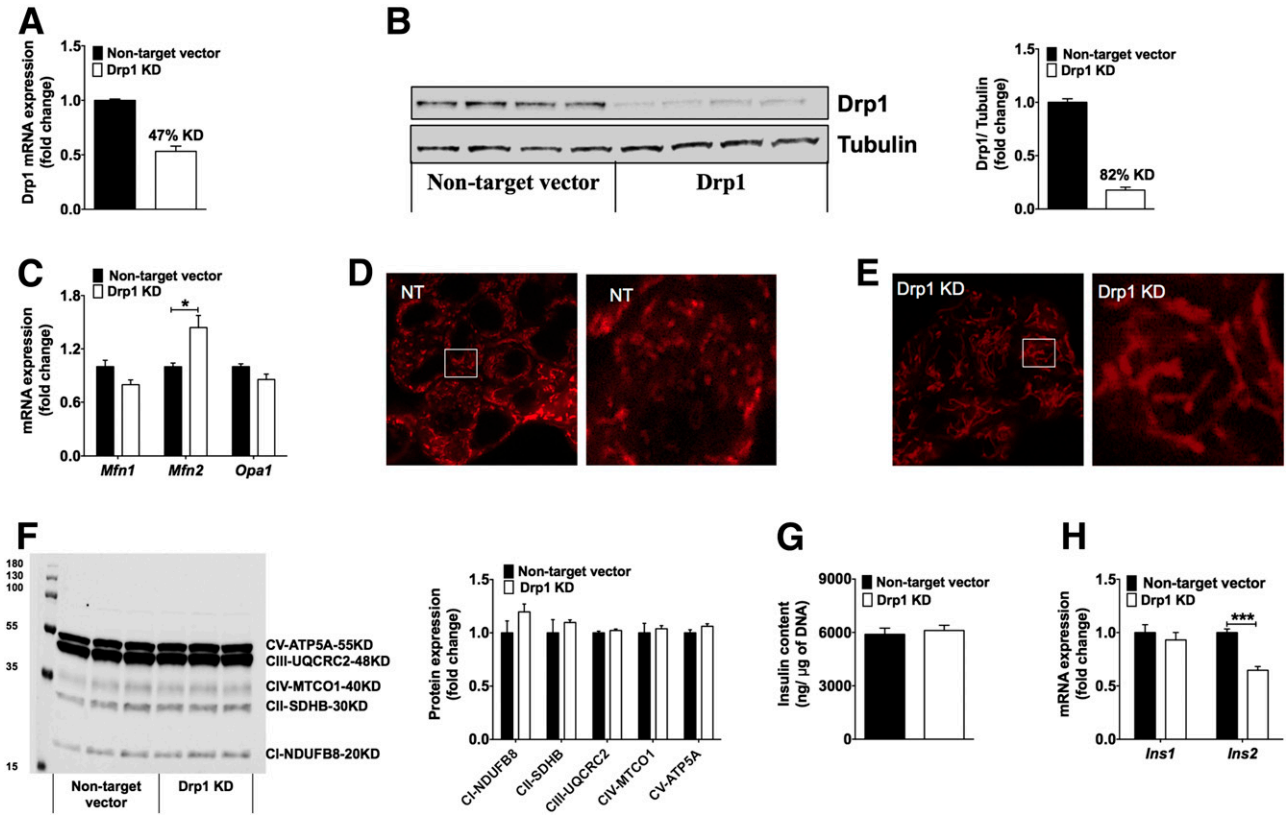

Figure 1—*A* and *B*: Knockdown of *Drp1* using lentiviral expression vectors. MIN6 cells were infected with nontarget vector (black bars) or *Drp1* shRNA (white bars) lentivirus and selected for stable cell lines. *A*: Knockdown efficiency was confirmed by quantitative PCR. Data are represented as mean ± SEM (n = 3). *B*: Immunoblot and quantification of *Drp1* protein content. Tubulin was used as a loading control (n = 4). *C*: Relative levels of *Mfn1*, *Mfn2*, and *Opa1* mRNA were measured by quantitative real-time PCR after knockdown of *Drp1* in MIN6 cells. *HPRT* was used as a control for each sample. Data are represented as mean ± SEM (n = 3). *D* and *E*: Live confocal imaging of stably infected MIN6 cells that were stained with MitoTracker Red FM for 30 min. Representative confocal images of the nontargeted vector (NT; *D*) and *Drp1* KD cells (*E*). *F*: Immunoblot and densitometric quantification of protein from various oxidative phosphorylation subunits in *Drp1* KD vs. nontarget vector MIN6 cells (n = 3). *G*: Insulin content in *Drp*1 KD MIN6 cells measured with insulin ELISA. Data are represented as mean ± SEM (n = 4). *H*: Relative levels of *Ins1* and *Ins2* mRNA were measured by quantitative real-time PCR after knockdown of *Drp1* in MIN6 cells. *HPRT* was used as a control for each sample. Data are represented as mean ± SEM (n = 3), and n values represent independent experiments. Statistical significance of mean differences was tested by unpaired two-tailed Student t test. $^*P < 0.05$; $^{***}P < 0.001$.

between *Drp1* KD and control cells (Fig. 2*C*), although glucose-stimulated respiration tended to be lower in *Drp1* KD cells (Fig. 2*C*). Interestingly, *Drp1* depletion from MIN6 cells lowered mitochondrial respiration that is used to make ATP at high glucose (Fig. 2*D*), a statistically significant effect reflected by decreased coupling efficiency of glucose-stimulated oxidative phosphorylation (Fig. 2*E*). This relatively low coupling efficiency also reflects an increase in mitochondrial proton leak that is provoked by *Drp1* KD at high glucose (Fig. 2*F*). Note that the concomitant changes in oxygen consumption linked to proton leak (increase) and ATP synthesis (decrease) neutralize each other, such that overall glucose-stimulated respiration does not differ significantly between *Drp1* KD and control cells (Fig. 2*C*). Because the bioenergetic effects of *Drp1* depletion are not caused by changes in respiratory chain components (Supplementary Fig. 1), impaired GSIS in the MIN6 cells upon *Drp1* KD is thus directly related to the decreased rate and coupling efficiency of glucose-stimulated oxidative phosphorylation. Consistently, *Drp1* KD decreases intracellular ATP content upon glucose stimulation by ~30% (Fig. 2*G*).

Pharmacological Drp1 Inhibition Corroborates the Genetic *Drp1* KD Phenotype

Long-term genetic inactivation of *Drp1* may well affect mitophagy and mitochondrial quality control, which confounds interpretation of *Drp1* KD effects on GSIS. Indeed, gene expression changes in the *Drp1* KD model suggest cellular adaptation (Fig. 1*C* and *H*), which is why we examined whether acute selective, chemical inhibition of *Drp1* that recapitulates the reduction of GSIS impairment is caused by genetic *Drp1* silencing. The cell-permeant, small molecule mdivi-1 inhibits *Drp1* assembly and GTPase activity and has been previously suggested as a therapeutic for stroke, myocardial infarction, and neurodegenerative diseases (26–29). We preincubated MIN6 cells with 25 or 50 µmol/L mdivi-1 at basal and stimulatory glucose levels and found that mdivi-1 has no effect on insulin content

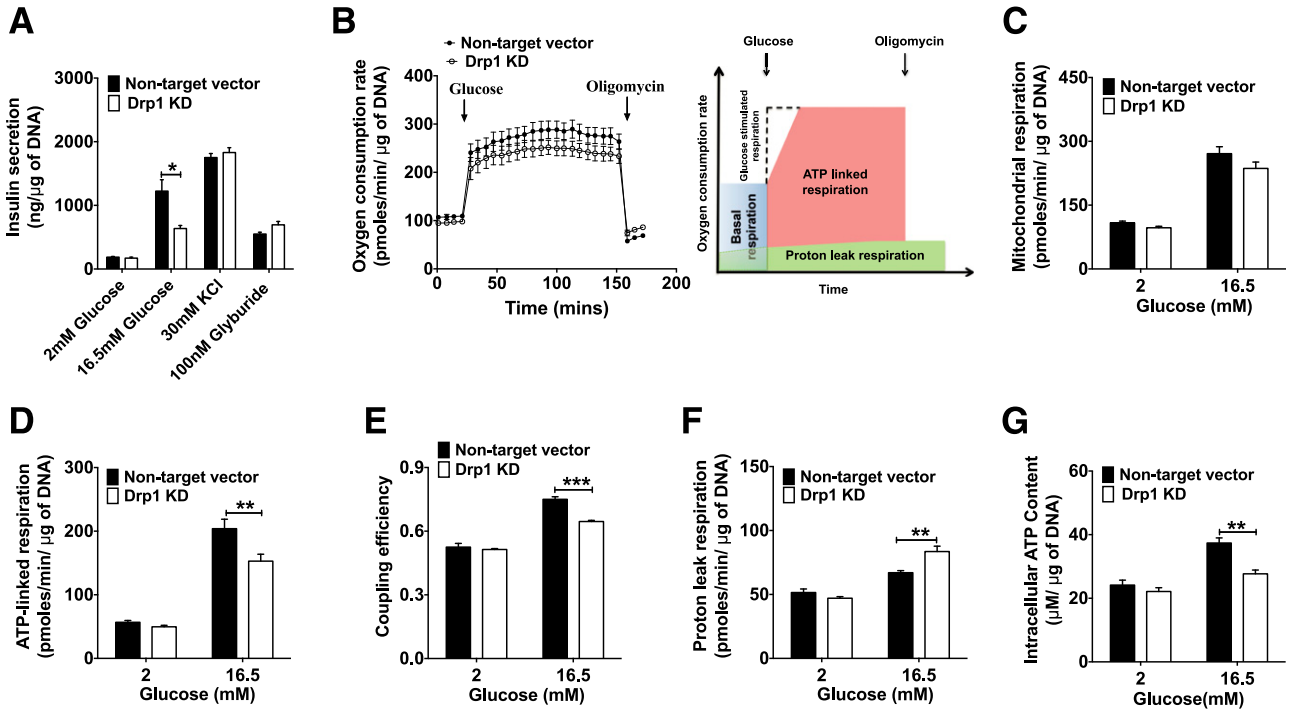

Figure 2—GSIS and bioenergetics of MIN6 cells. MIN6 cells stably infected with nontarget vector (black bars) and *Drp1* shRNA (white bars) lentivirus were exposed to either 2 or 16.5 mmol/L glucose. *A*: Insulin release was measured after 2 h in the presence of different secretagogues. Data are represented as mean ± SEM (n = 4). *B*: Averaged time-resolved oxygen consumption traces measured using the XF24 extracellular flux analyzer as described in RESEARCH DESIGN AND METHODS (left panel) and schematic representation marking different oxygen-consumption modules (right panel). *C*: Mitochondrial respiration in response to 2 and 16.5 mmol/L glucose. *D*: ATP-linked respiration. *E*: Coupling efficiency. Proton leak respiration (*F*) and ATP content (*G*). Data are represented as mean ± SEM (n = 6; n = 4 for *G*), and n values represent independent experiments. Statistical significance of mean differences was tested by unpaired two-tailed Student t test. *$P < 0.05$; **$P < 0.01$; ***$P < 0.001$.

(Fig. 3*A*) or basal insulin release (Fig. 3*B*). GSIS, however, is dose-dependently lowered by mdivi-1, reaching statistical significance at 50 μmol/L (Fig. 3*B*). These mdivi-1 effects echo those observed after *Drp1* KD (Fig. 2*A*). Equally, mdivi-1 fully mimicked the bioenergetic effects of *Drp1* KD: basal and glucose-stimulated respiration was unaffected by 50 μmol/L mdivi-1 (Fig. 3*C*), whereas mitochondrial proton leak was increased (Fig. 3*D*), and respiration used to make ATP was decreased (Fig. 3*E*). Consequently, mdivi-1 blunts the coupling efficiency of glucose-stimulated oxidative phosphorylation (Fig. 3*F*). Increasing the mdivi-1 dose to 100 μmol/L had no further impact on the bioenergetics of the MIN6 cells, suggesting that 50 μmol/L represents the fully inhibitory dose (Supplementary Fig. 2). To investigate the translational potential of fission-dependent GSIS, we incubated human pancreatic islets with mdivi-1 and, consistent with the cellular data, observed no effect on insulin content or basal insulin release but saw a significant decrease of GSIS (Fig. 4*A–C*). These results collectively demonstrate that inhibition of *Drp1*-mediated mitochondrial fission by mdivi-1 controls GSIS in both human pancreatic islets and cultured β-cells.

Mdivi-1 Decreases GSIS in Pancreatic Islets by Decreasing Oxidative Capacity

To explore the physiological and pathological relevance of *Drp1*, we studied the effect of mdivi-1 treatment on islets isolated from mice. Consistent with human islet and MIN6 cell data, mdivi-1 did not alter insulin content but attenuated GSIS (Fig. 4*D–F*). Representative real-time respiratory measurements under control conditions in islet-capture plates are depicted in Fig. 4*G* (see RESEARCH DESIGN AND METHODS). Mdivi-1 did not affect basal islet respiration at the low glucose concentration but significantly lowered glucose-stimulated respiration at the higher concentration (Fig. 4*H*). The lowered respiratory activity at high glucose was because of an mdivi-1–induced decrease of respiration linked to ATP synthesis (Fig. 4*I*), consistent with our results in MIN6 cells. Unlike its effect on cells, however, mdivi-1 left islet proton leak unaffected (Fig. 4*J*), which is why its inhibitory effect on ATP synthesis–coupled respiration is apparent from the overall glucose-stimulated oxygen consumption in islets (Fig. 4*H*). Consequent to its lowering effect on glucose oxidation linked to ATP synthesis, mdivi-1 significantly decreased the coupling efficiency of mouse islets (Fig. 4*K*). Collectively, these data demonstrate that *Drp1* controls islet GSIS by regulating glucose oxidation and not proton leak.

Pyruvate Rescues Impaired Function of Drp1-Deficient Cells and Islets

We hypothesized that the impaired glucose oxidation is likely secondary to reduced mitochondrial substrate supply, and we assessed this by directly providing pyruvate to mitochondria. We observed that the impaired

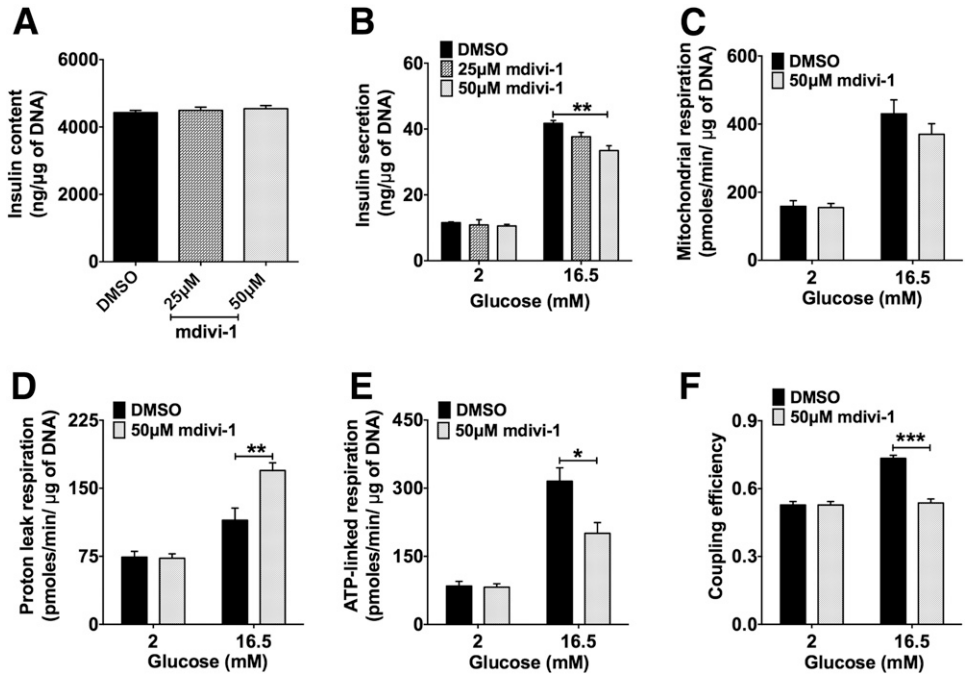

Figure 3—Mdivi-1 effects in MIN6 cell culture. *A–F*: MIN6 cells were exposed to either 2 or 16.5 mmol/L glucose with or without mdivi-1. *A*: Insulin content at different doses of mdivi-1. *B*: Insulin release at different doses of mdivi-1. Data are represented as mean ± SEM (n = 4). *C*: Mitochondrial respiration. *D*: Proton leak respiration. ATP-linked respiration (*E*) and coupling efficiency (*F*). Data are represented as mean ± SEM (n = 5), and n values represent independent experiments. Statistical significance of mean differences was tested by unpaired two-tailed Student t test to compare two variables, and one-way ANOVA (with Bonferroni post hoc analysis) was used for multiple comparisons. $^{*}P < 0.05$; $^{**}P < 0.01$; $^{***}P < 0.001$.

GSIS of *Drp1*-depleted MIN6 cells could be entirely rescued by supplying the cells with exogenous pyruvate (Fig. 5*A* and *B*). This observation suggests that pyruvate either circumvents defects in glucose-fueled ATP production or else triggers insulin secretion downstream of mitochondria. Pyruvate augments glucose-stimulated oxygen uptake in MIN6 cells irrespective of the presence of *Drp1* (Fig. 5*C*). The stimulatory effect of pyruvate on glucose oxidation was mirrored by a (not statistically significant) boost of GSIS in control and *Drp1*-depleted cells (Fig. 5*A*). Pyruvate stimulation restores ATP synthesis–linked respiration in *Drp1*-deficient cells to the level seen in control cells incubated at high glucose (Fig. 5*D*). The restorative effect of pyruvate is not evident from coupling efficiency (Fig. 5*E*), which remained low after pyruvate supplementation because of the persistently high mitochondrial proton leak exhibited by *Drp1* KD cells (Fig. 5*F*). Pyruvate thus rescues GSIS despite relatively high proton leak activity, demonstrating that GSIS impairment in *Drp1*-deficient cells is predominantly caused by decreased ATP synthesis ability. This conclusion is supported by the increased ATP content in pyruvate-treated cells (Fig. 5*G* and *H*). The restored ATP levels suggest that glucose-fueled oxidative phosphorylation in *Drp1*-deficient MIN6 cells is limited upstream of pyruvate (i.e., at the level of glycolysis). Glucose transporter gene expression and glucose uptake are not negatively affected in *Drp1* KD cells (Fig. 5*I* and *J*), and positive trends suggest deficiencies downstream of glucose transport. Interestingly, the use of glucokinase activator GKA50 improved glucose oxidation in *Drp1* KD cells and rescued GSIS (Fig. 5*K* and *L*).

It is difficult to gauge the translational potential of this pyruvate effect, as native β-cells lack the monocarboxylate carrier protein that allows insulinoma cells to take up pyruvate (1). Therefore, we tested the effect of pyruvate supplementation on mouse pancreatic islets treated with mdivi-1. GSIS deficiency was not rescued by sodium pyruvate in mouse pancreatic islets (Fig. 6*A* and *B*), thus excluding the possibility that pyruvate acts as an extracellular secretagogue that enhances secretory mechanisms downstream of mitochondria. However, GSIS impairment was entirely overcome by the membrane-permeant methyl pyruvate (Fig. 6*A* and *B*). Indeed, methyl pyruvate is also able to provoke insulin secretion in *Drp1*-inhibited mouse islets in the absence of glucose. One-hour incubation with methyl pyruvate fully rescued the *Drp1*-dependent deficiency of triggered insulin secretion in the presence and absence of 16.5 mmol/L glucose (Fig. 6*A*). The respective respiration measurements indicate that methyl pyruvate acts as a mitochondrial substrate by increasing mitochondrial respiration (Fig. 6*C*). Despite some increase in proton leak respiration when glucose and methyl pyruvate are combined (Fig. 6*D*), methyl pyruvate treatment overcomes Drp1-dependent differences in ATP

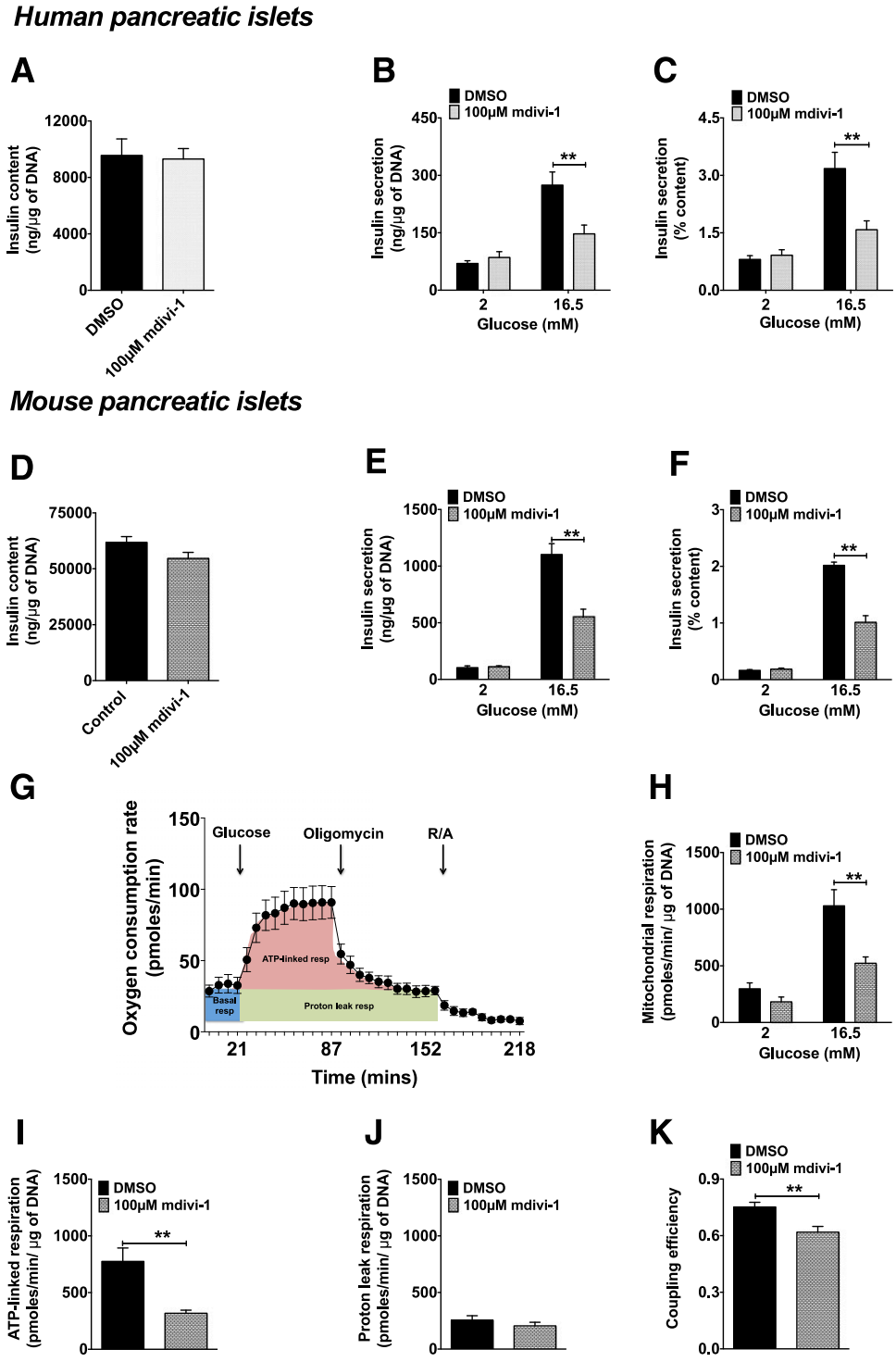

Figure 4— Mdivi-1 action on insulin secretion and mitochondrial bioenergetics in pancreatic islets. *A–C*: Human pancreatic islets were incubated with 2 and 16.5 mmol/L glucose with or without mdivi-1. Insulin content (*A*), insulin secretion (*B*), and insulin secretion normalized to insulin content (*C*) are depicted. *D–K*: Mouse pancreatic islets: batches of eight size-matched islets were exposed to either 2 or 16.5 mmol/L glucose with or without mdivi-1 (*D–F*). After incubation, supernatant and lysates were collected for insulin content (*D*), insulin secretion (*E*), and insulin secretion normalized to insulin content (*F*). Data are represented as means ± SEM of three independent experiments ($n = 3$). *G*: Representative scheme of time-resolved oxygen consumption traces of mouse wild-type pancreatic islets using islet-capture plates of the XF24 extracellular flux analyzer. *H*: Mitochondrial respiration at low (2 mmol/L) and high (16.5 mmol/L) glucose. *I*: ATP-linked respiration. Proton leak respiration (*J*) and coupling efficiency (*K*). Data are represented as means ± SEM ($n = 5$), and *n* values represent independent experiments. Statistical significance of mean differences was tested by unpaired two-tailed Student *t* test. $^{**}P < 0.01$. R/A, rotenone/antimycin A.

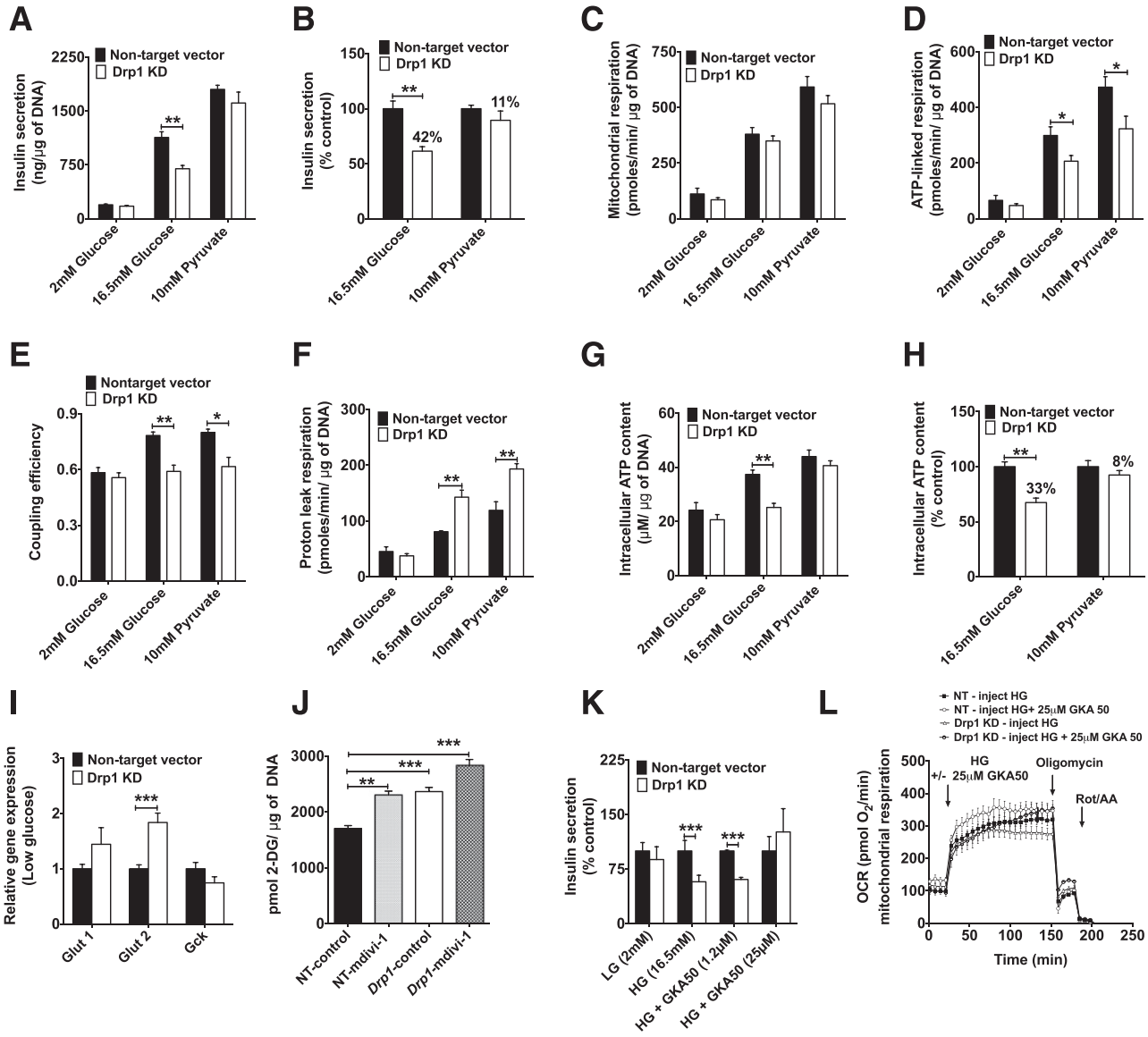

Figure 5—Pyruvate rescues *Drp1*-related deficiency in insulin secretion and bioenergetics in MIN6 cells. *A–H*: MIN6 cells with nontarget vector (black bars) and *Drp1* shRNA (white bars) lentivirus were exposed to glucose (2 and 16.5 mmol/L) or sodium pyruvate (10 mmol/L) for 2 h. *A*: Insulin secretion. *B*: Insulin secretion expressed as percentage of nontarget vector (control). *C*: Mitochondrial respiration. *D*: ATP-linked respiration. *E*: Coupling efficiency. *F*: Proton leak respiration. *G*: Intracellular ATP content. *H*: Intracellular ATP content expressed as percentage of nontarget vector (control). *I*: Relative levels of *Glut1*, *Glut2*, and *Gck* mRNA were measured by quantitative real-time PCR in wild-type and *Drp1* KD MIN6 cells. *HPRT* was used as housekeeping gene. *J*: Glucose uptake of MIN6 cells. *K* and *L*: Effect of glucokinase activator GKA50 on insulin secretion (*K*) and oxygen consumption rates (OCR; *L*). Data are represented as means ± SEM ($n = 4$), and n values represent independent experiments. Statistical significance of mean differences was tested by unpaired two-tailed Student t test to compare two variables, and one-way ANOVA (with Bonferroni post hoc analysis) was used for multiple comparisons. $^*P < 0.05$; $^{**}P < 0.01$; $^{***}P < 0.001$. HG, high glucose; LG, low glucose; NT, nontarget; Rot/AA, rotenone/antimycin A.

synthesis–linked respiration (Fig. 6*E*). Moreover, the mdivi-1–invoked difference in coupling efficiency is ameliorated by methyl pyruvate treatment (Fig. 6*F*). These findings suggest a model (Fig. 6*G*) that predicts that direct substrate delivery to mitochondria may be pursued as a potential route for drug intervention to rescue fission-impaired GSIS.

DISCUSSION

The present findings provide important insight into the mechanism by which the mitochondrial fission protein *Drp1* controls pancreatic insulin secretion. Specifically, the data demonstrate that *Drp1*-mediated mitochondrial fragmentation ensures that mitochondria are supplied with sufficient reducing power during GSIS. We demonstrate that *Drp1* deficiency does not directly impair glucose-stimulated oxidative phosphorylation, but instead limits mitochondrial ATP synthesis by compromising substrate delivery upstream of mitochondria. Unexpectedly, this limitation can be simply overcome by providing β-cells with exogenous pyruvate. This insight improves

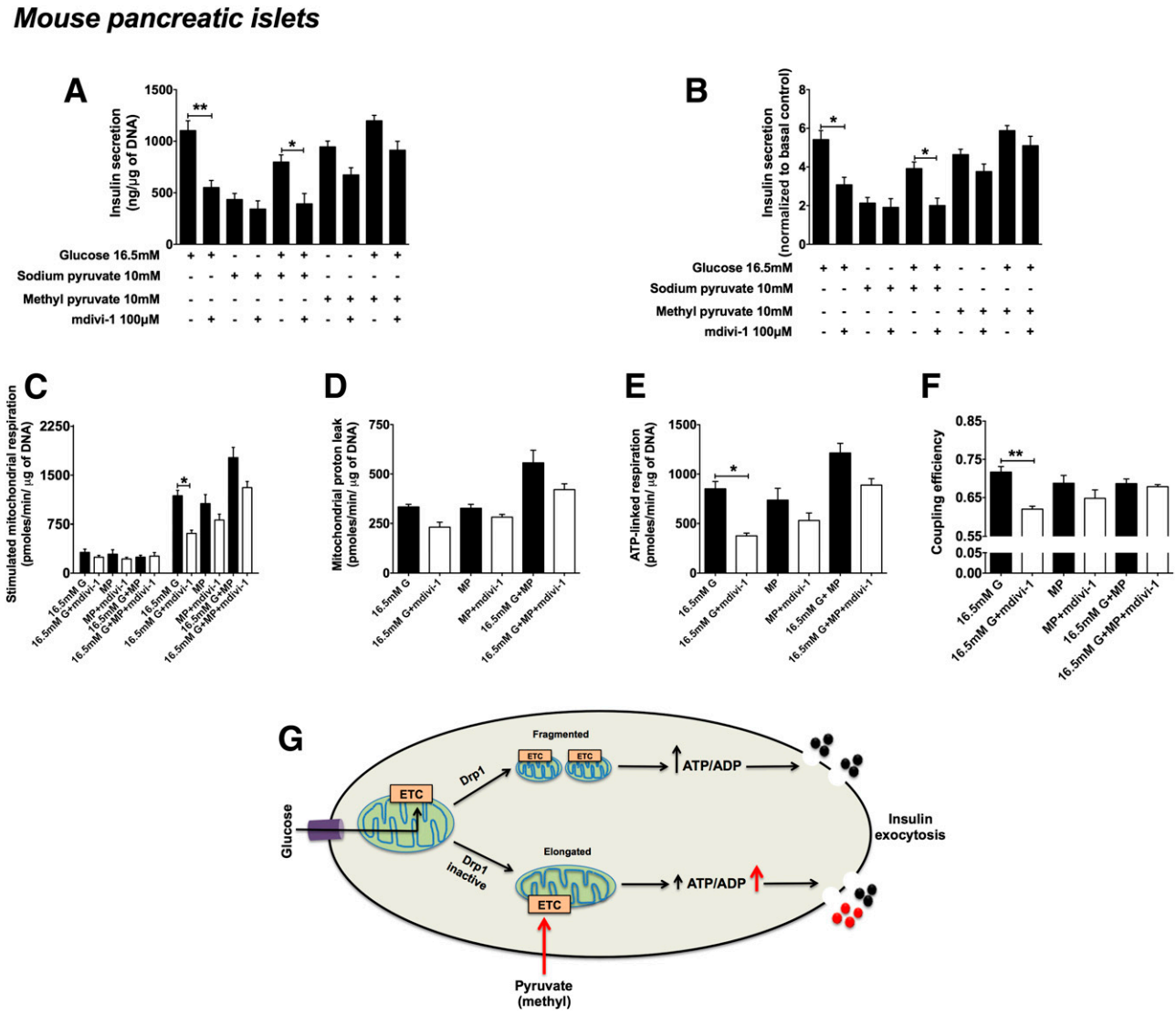

Figure 6—Methyl pyruvate rescues *Drp1*-related deficiency in insulin secretion and bioenergetics in pancreatic mouse islets. *A* and *B*: Batches of eight size-matched islets were exposed to different substrates/secretagogues with or without mdivi-1. After incubation, supernatant was collected to measure insulin secretion (*A*) and insulin secretion normalized to basal control (*B*). Data are represented as means ± SEM (n = 3). *C*: Mitochondrial respiration. *D*: Proton leak respiration. ATP-linked respiration (*E*) and coupling efficiency (*F*). *G*: Schematic model of the impact of *Drp1* during GSIS, emphasizing the rescue of insulin secretion with pyruvate. Statistical significance of mean differences was tested by unpaired two-tailed Student *t* test to compare two variables, and one-way ANOVA (with Bonferroni post hoc analysis) was used for multiple comparisons. $^*P < 0.05$; $^{**}P < 0.01$. ETC, electron transport chain; G, glucose; MP, methyl pyruvate.

our basic understanding of the relationship between mitochondrial dynamics and function (30), as it demonstrates that mitochondrial morphology can influence bioenergetic processes (glycolysis) that operate outside and upstream from the organelle itself. The ability to rescue impaired mitochondrial ATP output by direct substrate delivery opens a new window for the development of compounds to treat mitochondrial disorders and, more specifically, defects in insulin secretion associated with mitochondrial dysfunction.

Consistent with previous observations in INS-1E rat insulinoma cells overexpressing dominant-negative *Drp1* (22), we found that *Drp1* deficiency, due to either genetic knockdown or pharmacological inhibition, lowers GSIS in MIN6 mouse insulinoma cells. This *Drp1*-deficiency phenotype was also exhibited by mouse and human pancreatic islets, thus highlighting the physiological and translational relevance of *Drp1* control over GSIS. In agreement with the INS-1E cell data (22), we found that *Drp1* depletion from MIN6 cells increases mitochondrial respiration linked to proton leak and thus lowers coupling efficiency of oxidative phosphorylation. However, our plate-based respirometry analysis of adherent MIN6 cells disclosed that *Drp1* KD also causes a decrease of ATP synthesis–coupled respiration, an effect that contributes to the relatively low coupling efficiency in *Drp1*-depleted cells. Our experiments thus demonstrate that *Drp1* impacts both glucose-fueled respiration used to make ATP

and drive proton leak. In a more physiologically relevant experimental model, the pancreatic mouse islet, we further found that *Drp1* inhibition resulted in marked reduction of ATP synthesis–linked glucose oxidation without having an effect on proton leak. The islet data thus suggest that limited glucose-driven respiratory flux is the main explanation for impaired GSIS after *Drp1* inhibition rather than the increased proton leak that coincides with such limitation in cells. Indeed, our substrate rescue experiments demonstrate that the GSIS defects exhibited by mitochondrial fission–deficient MIN6 cells can be entirely overcome by pyruvate supplementation, despite the persistently elevated proton leak. Our data thus provide compelling evidence that glucose-stimulated oxidative phosphorylation in mitochondrial fission–deficient β-cells is largely controlled by mitochondrial substrate delivery, as pyruvate supplementation rescues respiration, ATP output, and insulin secretion, all of which were compromised after *Drp1* silencing. Similarly, cell-permeant methyl pyruvate rescues respiration, coupling efficiency, and insulin secretion in mdivi-1–treated islets. Further work, possibly involving global metabolomics approaches, is required on the crucial rate-limiting steps of substrate supply. Our study excludes compromised glucose availability, as glucose uptake was increased, not decreased, in *Drp1* KD cells. Interestingly, glucokinase activator GKA50 rescued respiration and insulin secretion in MIN6 cells, an observation that supports the concept of lowered glucose catabolism but that requires experimental confirmation in pancreatic islets. Future studies should also consider compromised shuttling of glycolytic NADH to the mitochondrial matrix. Although the rescue by pyruvate argues against a role for the mitochondrial pyruvate carrier during limited substrate supply in *Drp1*-deficient systems, restricted pyruvate transport can also not be formally excluded at this stage.

Our experiments highlight how modern technologies for measuring cellular and islet bioenergetics (such as real-time multiwell plate–based respirometry) improve our understanding of insulin secretion in pancreatic β-cells. Nutrient–secretion coupling depends to a large degree on the link between glucose catabolism and ATP-triggered signaling events that lead to the exocytosis of insulin-containing granules. The strength of nutrient–secretion coupling is largely determined by the extent to which energy liberated during glucose combustion is used to make ATP and by how much of it is wasted via mitochondrial proton leak. Coupling efficiency of oxidative phosphorylation is an often-underestimated bioenergetic parameter that is highly critical for β-cell biology, as it quantifies the proportion of glucose-fueled respiration that is coupled to ATP synthesis. As coupling efficiency is an internally normalized parameter, it benefits from a comparably high signal-to-noise ratio that renders it exquisitely sensitive to any perturbation in proton leak, mitochondrial ATP synthesis, and/or cellular substrate oxidation (31). Indeed, changes in coupling efficiency following *Drp1* silencing underpin our discovery that glycolytic substrate delivery to mitochondria is the single parameter that controls insulin secretion, whereas direct effects on energy transduction (proton leak) play a minor role.

Other players in the mitochondrial fission–fusion system, such as *Opa1* (32), also have profound effects on GSIS. Whether or not these effects can be neutralized by substrate supplementation or stimulation of fusion genes such as mitofusin (*Mfn*), or if pathological changes in mitochondrial dynamics may more generally be rescued by increased substrate delivery, are questions that should be considered for future studies. In this respect, it has recently been reported that cellular energy deficiency induces mitochondrial fission via *AMPK*-dependent *Fis1* and *Drp1* recruitment (33). This fission has been interpreted as being prerequisite for the removal of faulty mitochondria by mitophagy (33), but our findings offer the alternative possibility that mitochondrial fragmentation enhances glycolytic metabolite delivery to mitochondria and thus maintains ATP output during times of high energetic demand. In conclusion, mitochondrial dynamics exert profound control over cellular bioenergetics and, although influencing mitochondrial activity per se, also affect upstream energetic processes such as substrate delivery.

Acknowledgments. The authors thank Ruchi Jain and Maria Kutschke at the Helmholtz Zentrum München for excellent technical assistance and the ECIT for providing human islets.

Funding. This work was supported in part by funding from the German Center for Diabetes Research (to M.J.), the Alexander von Humboldt Foundation (to M.H.T.), and the Helmholtz Alliance ICEMED–Imaging and Curing Environmental Metabolic Diseases through the Initiative and Networking Fund of the Helmholtz Association and the Helmholtz cross-program topic "Metabolic Dysfunction." O.K. and H.L. have received funding for the HumEn project from the European Union's Seventh Framework Programme for Research, Technological Development and Demonstration, under grant 602587 (http://www.hum-en.eu/). Human islets were provided by JDRF under award 31-2008-416 (ECIT Islets for Basic Research Program).

Duality of Interest. No potential conflicts of interest relevant to this article were reported.

Author Contributions. U.D.K. and M.J. conceptualized the research plan and analyzed all results. U.D.K. conducted most cell culture and mouse experiments. K.P. conducted the perfusion of mice for islet isolation. A.M. conducted the experiments with human islets. S.K. performed cell culture experiments. D.L. performed seahorse experiments and glucose uptake. O.K. provided human islets. M.G. advised on microscopic experiments. U.D.K., S.K., S.C.W., C.A., and M.J. interpreted all experiments and wrote the manuscript. P.T.P., H.L., and M.H.T. contributed reagents, materials, or analytic tools and gave advice on experimental design. M.J. is the guarantor of this work and, as such, had full access to all the data in the study and takes responsibility for the integrity of the data and the accuracy of the data analysis.

References

1. Rutter GA, Pullen TJ, Hodson DJ, Martinez-Sanchez A. Pancreatic β-cell identity, glucose sensing and the control of insulin secretion. Biochem J 2015; 466:203–218

2. Ashcroft FM, Proks P, Smith PA, Ammälä C, Bokvist K, Rorsman P. Stimulus-secretion coupling in pancreatic beta cells. J Cell Biochem 1994;55(Suppl.):54–65

3. Maechler P, Li N, Casimir M, Vetterli L, Frigerio F, Brun T. Role of mitochondria in beta-cell function and dysfunction. Adv Exp Med Biol 2010;654:193–216

4. Molina AJ, Wikstrom JD, Stiles L, et al. Mitochondrial networking protects beta-cells from nutrient-induced apoptosis. Diabetes 2009;58:2303–2315
5. Chan DC. Mitochondria: dynamic organelles in disease, aging, and development. Cell 2006;125:1241–1252
6. Hoppins S, Lackner L, Nunnari J. The machines that divide and fuse mitochondria. Annu Rev Biochem 2007;76:751–780
7. Chan DC. Fusion and fission: interlinked processes critical for mitochondrial health. Annu Rev Genet 2012;46:265–287
8. Chen H, Chan DC. Emerging functions of mammalian mitochondrial fusion and fission. Hum Mol Genet 2005;14:R283–R289
9. Mishra P, Chan DC. Metabolic regulation of mitochondrial dynamics. J Cell Biol 2016;212:379–387
10. Alexander C, Votruba M, Pesch UE, et al. OPA1, encoding a dynamin-related GTPase, is mutated in autosomal dominant optic atrophy linked to chromosome 3q28. Nat Genet 2000;26:211–215
11. Waterham HR, Koster J, van Roermund CW, Mooyer PA, Wanders RJ, Leonard JV. A lethal defect of mitochondrial and peroxisomal fission. N Engl J Med 2007;356:1736–1741
12. Züchner S, Mersiyanova IV, Muglia M, et al. Mutations in the mitochondrial GTPase mitofusin 2 cause Charcot-Marie-Tooth neuropathy type 2A [published correction appears in Nat Genet 2004;36:660]. Nat Genet 2004;36:449–451
13. Anello M, Lupi R, Spampinato D, et al. Functional and morphological alterations of mitochondria in pancreatic beta cells from type 2 diabetic patients. Diabetologia 2005;48:282–289
14. Smirnova E, Griparic L, Shurland DL, van der Bliek AM. Dynamin-related protein Drp1 is required for mitochondrial division in mammalian cells. Mol Biol Cell 2001;12:2245–2256
15. Lackner LL, Nunnari JM. The molecular mechanism and cellular functions of mitochondrial division. Biochim Biophys Acta 2009;1792:1138–1144
16. Chang CR, Blackstone C. Drp1 phosphorylation and mitochondrial regulation. EMBO Rep 2007;8:1088–1089; author reply 1089–1090
17. Santel A, Frank S. Shaping mitochondria: the complex posttranslational regulation of the mitochondrial fission protein DRP1. IUBMB Life 2008;60:448–455
18. Liu J, Chen Z, Zhang Y, et al. Rhein protects pancreatic β-cells from dynamin-related protein-1–mediated mitochondrial fission and cell apoptosis under hyperglycemia. Diabetes 2013;62:3927–3935
19. Men X, Wang H, Li M, et al. Dynamin-related protein 1 mediates high glucose induced pancreatic beta cell apoptosis. Int J Biochem Cell Biol 2009;41:879–890
20. Peng L, Men X, Zhang W, et al. Involvement of dynamin-related protein 1 in free fatty acid-induced INS-1-derived cell apoptosis. PLoS One 2012;7:e49258
21. Peng L, Men X, Zhang W, et al. Dynamin-related protein 1 is implicated in endoplasmic reticulum stress-induced pancreatic β-cell apoptosis. Int J Mol Med 2011;28:161–169
22. Jhun BS, Lee H, Jin ZG, Yoon Y. Glucose stimulation induces dynamic change of mitochondrial morphology to promote insulin secretion in the insulinoma cell line INS-1E. PLoS One 2013;8:e60810
23. Carter JD, Dula SB, Corbin KL, Wu R, Nunemaker CS. A practical guide to rodent islet isolation and assessment. Biol Proced Online 2009;11:3–31
24. Divakaruni AS, Paradyse A, Ferrick DA, Murphy AN, Jastroch M. Analysis and interpretation of microplate-based oxygen consumption and pH data. Methods Enzymol 2014;547:309–354
25. Affourtit C, Brand MD. Measuring mitochondrial bioenergetics in INS-1E insulinoma cells. Methods Enzymol 2009;457:405–424
26. Lackner LL, Nunnari J. Small molecule inhibitors of mitochondrial division: tools that translate basic biological research into medicine. Chem Biol 2010;17:578–583
27. Manczak M, Reddy PH. Mitochondrial division inhibitor 1 protects against mutant huntingtin-induced abnormal mitochondrial dynamics and neuronal damage in Huntington's disease. Hum Mol Genet 2015;24:7308–7325
28. Zaja I, Bai X, Liu Y, et al. Cdk1, PKCδ and calcineurin-mediated Drp1 pathway contributes to mitochondrial fission-induced cardiomyocyte death. Biochem Biophys Res Commun 2014;453:710–721
29. Zhao YX, Cui M, Chen SF, Dong Q, Liu XY. Amelioration of ischemic mitochondrial injury and Bax-dependent outer membrane permeabilization by Mdivi-1. CNS Neurosci Ther 2014;20:528–538
30. Liesa M, Shirihai OS. Mitochondrial dynamics in the regulation of nutrient utilization and energy expenditure. Cell Metab 2013;17:491–506
31. Brand MD, Nicholls DG. Assessing mitochondrial dysfunction in cells. Biochem J 2011;435:297–312
32. Zhang Z, Wakabayashi N, Wakabayashi J, et al. The dynamin-related GTPase Opa1 is required for glucose-stimulated ATP production in pancreatic beta cells. Mol Biol Cell 2011;22:2235–2245
33. Toyama EQ, Herzig S, Courchet J, et al. Metabolism. AMP-activated protein kinase mediates mitochondrial fission in response to energy stress. Science 2016;351:275–281